Early Events in Apomyoglobin Unfolding Probed by Laser T-jump/UV Resonance Raman Spectroscopy†

Cheng-Yen Huang, Gurusamy Balakrishnan, and Thomas G. Spiro*

Department of Chemistry, Princeton University, Princeton, New Jersey 08544

Received August 9, 2005; Revised Manuscript Received September 16, 2005

ABSTRACT: Early events in the unfolding of apomyoglobin are studied with time-resolved ultraviolet resonance Raman (UVRR) spectroscopy coupled to a laser-induced temperature jump (T-jump). The UVRR spectra provide simultaneous probes of the aromatic side-chain environment and the amide backbone conformation. The amide bands reveal helix melting, with relaxation times of 70 and 16 μs at pH 5.5 and 4, respectively, in reasonable agreement with previously reported amide I′ FTIR/T-jump relaxations (132 and 14 μs at pD 5.5 and 3). The acceleration at pH 4 is consistent with destabilization of the hydrophobic AGH core of the protein via protonation of a pair of buried histidines. The same relaxation times are found for intensity loss by the phenylalanine F12 band, signaling solvent exposure of the phenyl rings. There are seven Phe residues, distributed throughout the protein; they produce a global response, parallel to helix melting. Relaxation of the tryptophan W16 intensity also parallels helix melting at pH 5.5 but is twice as fast, 7 μs, at pH 4. The pH 5.5 signal arises from Trp 7, which is partially solvent-exposed, while the pH 4 signal arises from the buried Trp 14. Thus, Trp 14 is exposed to the solvent prior to helix melting of the AGH core, suggesting initial displacement of the A helix, upon which Trp 14 resides. All of the UVRR signals show a prompt response, within the instrument resolution (∼60 ns), which accounts for half of the total relaxation amplitude. This response is attributed to solvent penetration into the protein, possibly convoluted with melting of hydrated helix segments.

Laser-induced temperature-jump (T-jump)[1] technology has emerged as a general method for studying early events in protein folding and unfolding (*1*−*5*). In this technique, an infrared laser pulse, tuned to a vibrational overtone absorption band of H_2O or D_2O rapidly heats an aqueous solution, perturbing the structure of dissolved protein. The subsequent evolution of this structure can then be monitored by spectroscopic probes. Fluorescence (*3*, *4*), infrared (*1*, *2*), and Raman spectroscopy (*5*) have all been used in T-jump studies.

Raman spectroscopy holds particular promise because it can provide multiple structure markers in a single experiment. Excitation at ultraviolet wavelengths can selectively enhance vibrational modes of aromatic side chains (*6*) or of the main-chain amide bonds (*7*). The former are indicators of tertiary structure, while the latter can be used to assess secondary structure (*8*). The principal limitation is that the Raman signals are relatively weak, even with the benefit of resonance enhancement, and the small changes induced by a T-jump are difficult to measure accurately. Infrared signals can be measured with higher accuracy, but water is opaque in most of the relevant spectral region, and infrared (IR) studies of protein folding have thus far been limited to the amide I′ (C═O stretching) band in D_2O solution.

To facilitate T-jump/Raman studies, we have implemented a near-IR laser (OPO) with a 1 kHz repetition rate (*9*), coupled with a 1 kHz tunable UV Raman laser (frequency-quadrupled Ti:sapphire) (*10*−*12*). The high data rate of this system improves signal/noise, and the UV tunability permits optimization of selective resonance enhancement. The tuning range has been extended to 193 nm (*12*), and we have found that 197 nm excitation provides superior capture of amide Raman bands, facilitating secondary structure analysis (*13*).

In the present work, we apply this instrument to the unfolding dynamics of apomyoglobin (apoMb), a widely studied test system for protein-folding studies (*1*, *3*). NMR studies have shown that when the heme is removed from Mb, the native fold is preserved, except that the F helix, which holds the heme-ligating histidine residue, becomes disordered (Figure 1) (*14*, *15*). However, the structure is destabilized by the heme removal, and a variety of less ordered states can be accessed by adding protons or denaturing agents (*16*). When the pH is lowered to 4, the E, D, and C helices become disordered, as does part of the B helix, but a tightly packed core is retained, consisting of the A, G, and H helices and the C-terminal part of the B helix (Figure 1) (*17*). At pH 2, this core also unravels, although regions of fluctuating local structure can be detected. The pH 4 structure is essentially the same as that of an obligatory intermediate (I) on the protein-folding pathway (*18*, *19*).

Previous T-jump studies have documented rapid changes in apoMb. Infrared transients gave 48 ns and 132 μs time constants for the decay of amide I signals associated with

† This work was supported by the National Institutes of Health under Grant number GM 25158.

* To whom correspondence should be addressed. E-mail: spiro@princeton.edu. Telephone: (609) 258-3907. Fax: (609) 258-0348.

[1] Abbreviations: UVRR, ultraviolet resonance Raman; T-jump, temperature jump; IR, infrared; apoMb, apomyoglobin; CD, circular dichroism.

10.1021/bi051578u CCC: $30.25
Published on Web 11/05/2005

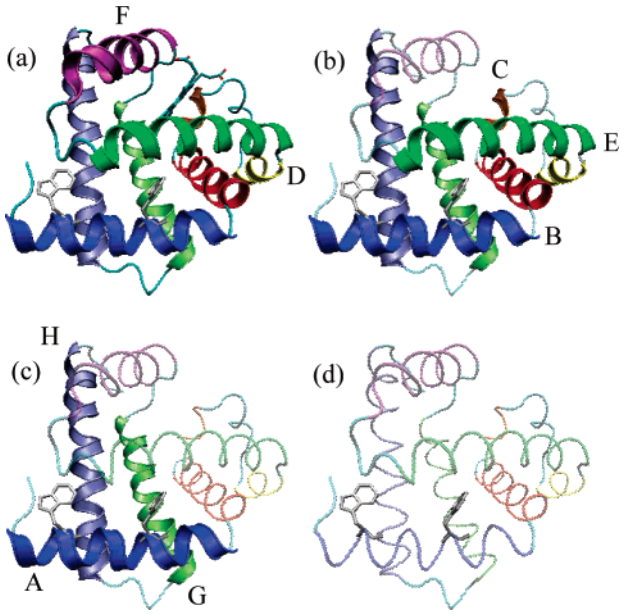

FIGURE 1: Ribbon diagram using VMD (*39*) for native Mb (a) (PDB 1AZI), successive melting of helices (light tubes) upon heme removal (b), and subsequent pH lowering to 4 (c) and 2 (d), on the basis of NMR (*18*). The A helix residues Trp 7 and Trp 14 are shown in gray.

solvated (1633 cm^{-1}) and native (1659 cm^{-1}) helices, respectively, in native apoMb (pD 5.5) (*1*). Tryptophan flouresence and amide I (1650 cm^{-1}) IR relaxations both gave 14 μs for the loss of the structure in a low pH intermediate (called E, pH 3 with low salt), which retains some of the AGH core (*20*). In addition, fluorescence relaxation has indicated that cold-denatured apoMb can regain the AGH core in less than 20 μs (*3*).

We find similar fast processes in native apoMb and the pH 4 intermediate via ultraviolet resonance Raman (UVRR) spectroscopy. The ability to compare amide and aromatic residue signals in the same experimental system permits more detailed structural interpretation.

MATERIALS AND METHODS

Materials. Horse heart myoglobin, phenylalanine, and tyrosine were purchased from Sigma (St. Louis, MO) and used without further purification. Apomyoglobin was prepared by 2-butanone extraction of horse heart myoglobin under acidic conditions (*21*, *22*). After heme extraction, the apoMb solution was dialyzed extensively against Milli-Q Millipore water (Billerica, MA) and then diluted with Millipore water to the desired sample concentration. The final pH of the sample was adjusted by slowly adding concentrated HCl solution. No extra salt was added, because apoMb tends to aggregate at high temperatures in the presence of salt. The final sample concentration was determined from the protein molar extinction coefficient, 14 620 M^{-1} cm^{-1} at 280 nm (*23*), using an Agilent 8453 UV−vis spectrophotometer. The residual heme was estimated to be less than 1% from the sample absorbance at 408 nm.

Circular Dichroism (CD) Measurements. Variable temperature far-UV CD wavelength scans were collected on an AVIV 62DS spectropolarimeter equipped with a temperature-controlled cuvette holder, using a 1 mm quartz cell. The data were recorded from 260 to 190 nm with 1 nm spacing and every 5 °C from 5 to 95 °C. The protein concentration was ~20 μM for both pH samples. The data were converted to mean residue ellipticity (θ) in deg cm^2/dmol using the measured protein concentration. Secondary structure analysis of the final CD data was carried out using the CONTINLL program in the CDPro software package (*24*).

Equilibrium UVRR Measurements. The experimental setup and the spectral acquisition scheme have previously been described. UV probe pulses (20 ns, 1 kHz) at 197 nm (*12*) (~1 μJ/pulse) or 229 nm (*10*, *11*) (~1 μJ/pulse) were obtained by frequency quadrupling of the output of a Ti:sapphire laser, which was pumped (527 nm, ~10 mJ/pulse, 70 ns, 1 kHz) by an intracavity frequency-doubled Nd:YLF laser (GM30, Photonics International, Inc.). Raman scattered light was collected at 135° geometry and focused into a 1.26 m spectrograph (Spex 1269), which was equipped with a holographic grating (3600 groove/mm) and an intensified photodiode array detector (IPAD) (Roper Scientific). The sample solution was pumped through a wire-guided free-flowing cell to minimize the background. Temperature control of the sample was achieved with a water bath (RTE-100, Neslab), which regulates the temperature of the sample cell and reservoir. UVRR spectra were collected with 15 min accumulation time. The measured spectra were calibrated using the Raman spectrum of cyclohexane. The water background was subtracted from protein Raman spectra using the pure water Raman spectrum.

Time-Resolved T-jump UVRR Measurements. UV probe pulses for time-resolved UVRR measurements were generated by the UV laser described above. T-jump pulses were obtained (*9*) from an intracavity diode laser pumped Nd:YLF laser optical parametric oscillator (OPO), which can generate tunable near-infrared (NIR) 1.8−2.0 μm, 0.8−1.0 mJ/pulse, 20 ns, 1 kHz pulses (Photonics International, Inc.). The final temperature of the sample after T-jump was determined to ±2 °C from the ~3400 cm^{-1} water Raman band intensity change. The frequency of the T-jump pump pulse is within the near-IR water band centered at 1.9 μm. The final temperature of the sample within the laser interaction volume is achieved instantaneously after T-jump pulse [complete thermalization is reached within ~10−20 ps (*25*)]. The probe and pump pulse sequence was alternated to minimize artifacts from spectrometer drift and photoproduct accumulation, which is critical for this study, because no internal standard was added. The timing between T-jump and probe pulses was adjusted with a computer-controlled pulse generator (DG 535, Stanford Research Systems). The final pump−probe (with T-jump) and probe-only (without T-jump) spectra were the averages over 15 min of accumulation.

RESULTS

Thermal Melting. The far-UV CD spectra (Figure 2) show features characteristic of α helices: negative peaks near 222 and 207 nm and a positive 193 nm peak. The amplitude is lower at pH 4 than 5.5, consistent with the expected partial unfolding. Analysis of the 25 °C spectra with the CONTINLL program (*24*) yielded helix fractions of 0.38 and 0.63 at pH 4.0 and 5.5, consistent with previous determinations (*18*). As the temperature increases, the helices melt (inset of Figure 2). A two-state fit to the data yields T_m values

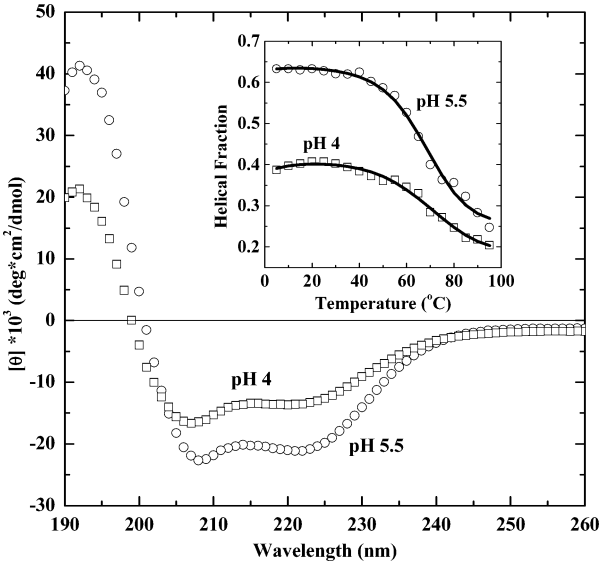

FIGURE 2: Far-UV CD spectra (25 °C) for apoMb at the indicated pH values. The inset shows helical fraction calculated [CONTINLL program in CDPro (*24*)] from variable temperature CD spectra. The solid lines are fits of the data to a two-state model with T_m = 67 °C (pH 5.5) and 56 °C (pH 4).

of 67 and 56 °C at pH 5.5 and 4, somewhat higher than previous determinations (*26*). The T_m values are sensitive to the presence of salts, which were avoided in the present study, to minimize precipitation at high temperatures. Although the CD melting curves are reasonably cooperative, considerable structure is retained, even at 95 °C, where the measured helix fractions are 0.25 and 0.20 at pH 5.5 and 4.0.

The 197-nm-excited UVRR spectra show temperature-dependent changes in amide band intensities, which are indicative of the loss in α-helix content (*13*), as seen in Figure 3. The temperature-difference spectra reveal intensities decreasing or increasing with the temperature at positions characteristic of helix and random coil, respectively (see the arrows). The spectra also contain bands arising from phenylalanine (F) and tyrosine (Y) residues. Their intensities decrease with temperature, indicating exposure of aromatic side chains to the solvent (see below). The same trend is seen in spectra excited at 229 nm (Figure 4), where bands of tryptophan (W) and tyrosine are selectively enhanced.

Intensity trends for well-isolated aromatic bands are plotted in Figure 5, along with intensities of the same bands from spectra of the aqueous aromatic amino acid. The latter show some temperature dependence, reflecting exposure of the aromatic groups to a changing environment of water hydrogen bonds. The biggest effect (20% drop in intensity between 10 and 90 °C) was shown by aqueous tyrosine, reflecting the importance of hydrogen bonding with the phenolic OH group. In all cases, the intensity loss for the apoMb band is greater than the aqueous amino acid background. This is the expected effect of exposing buried aromatic side chains to solvent H_2O. The one exception is the tyrosine Y1 band at pH 4, where the temperature dependence is about the same for apoMb as for aqueous tyrosine, suggesting that the side chains are fully exposed in the protein.

Because the addition of salt to the protein solutions was avoided, there is no internal intensity standard, making it impossible to scale the protein and aqueous amino acid intensities. The data in Figure 5 are plots of the intensity at a given temperature relative to the intensity at 90 °C, but the ratios for protein and aqueous amino acid signals would only be comparable if the protein side chains were fully exposed to the solvent at 90 °C, which may not be the case. Thus, only the trends in Figure 5 are meaningful.

To assess the helix content from the amide intensities in the 197 nm spectra, the aromatic contributions were suppressed by subtracting the aqueous amino acid spectra, using a strong isolated aromatic band (F12 at 1003 cm^{-1} for phenylalanine and Y1 at 853 cm^{-1} for tyrosine) for normalization (Figure 6). The subtraction is imperfect because the relative intensities for the various aromatic bands are somewhat dependent upon the environment, but it improves the fidelity to backbone conformation of amide bands adjacent to aromatic bands. The spectral regions containing the amide bands (1625−1750 cm^{-1}, amide I; 1475−1575 cm^{-1}, amide II; and 1225−1425 cm^{-1}, amide III and S) were then fit via least squares as described elsewhere (*13*) to determine helix and coil contents, using the measured protein concentrations for normalization. The resulting helical fractions are plotted in Figure 7 and compared with the fractions computed from the CD spectra. The agreement is seen to be quite satisfactory, although the UVRR plot at pH 5.5 is distinctly less cooperative, and retains a higher helical fraction at high temperatures. This difference reflects different helix-length dependencies of the two kinds of spectra. The CD signal depends upon excitonic interactions among chiral centers along a helix; the molar ellipticity diminishes for short helices (*27*). In contrast, the UVRR signal is localized on each amide unit and is sensitive to secondary structure mainly through the altered conformations of the amide bond (*28*). The higher helix fraction at high temperatures indicates the persistence of residual short α-helical units as the long helices unravel; the population of these short segments is underestimated in the CD spectra (*28*).

T-jumps. Figures 8 and 9 show difference spectra induced by laser T-jumps at pH 5.5 and 4.0, respectively. The changes are all in the directions expected from the thermal profiles (Figures 5 and 7), but the amplitudes are small, because the thermal profiles are gradual, and the T-jumps were modest, 40−60 °C at pH 5.5 and 45−60 °C at pH 4.0. Larger T-jumps were precluded by sample instability. Probe and pump−probe spectra were analyzed in the same way as the variable-temperature spectra, and the time profiles of the changes are given in Figures 10 and 11 for the helix content (197 nm spectra), the amplitude of the phenylalanine F12 band (197 nm spectra), and the amplitude of the tryptophan W16 band (229 nm spectra). We were unable to obtain a reliable time course for tyrosine, probably because of the modest strength of the tyrosine bands (Figures 3 and 4) and the small changes with temperature (Figure 5).

The time courses all show a fast initial drop in signal, which is within the time resolution of the experiment (estimated to be 60 ns, from the laser pulse widths and jitter), followed by a slower decrease, on the microsecond time scale. The slow phases were fit to exponential decays, with the indicated time constants. Because of the scatter in the data, the uncertainties in the time constants are substantial (Table 1). Nevertheless, it is clear that the time constants are ∼60 μs at pH 5.5 and 4−5 times shorter at pH 4. The uncertainties are lower at pH 4, and here, it seems clear that

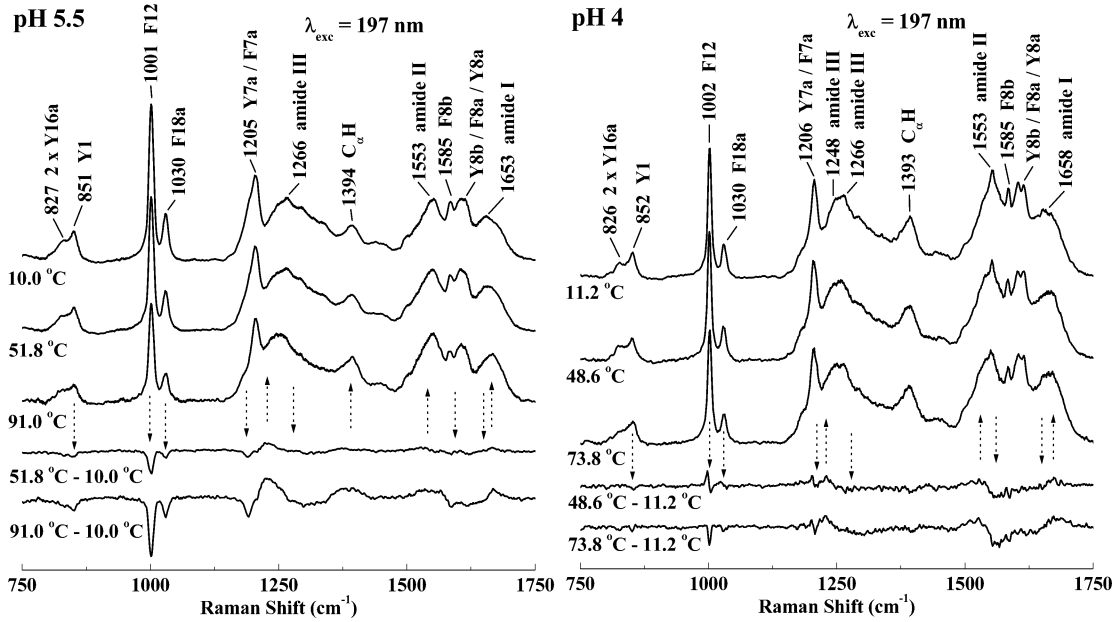

FIGURE 3: Variable temperature UVRR spectra of apoMb excited at 197 nm. Arrows mark the direction of intensity changes, as revealed in the difference spectra. Mode assignments are indicated at the top. A 197 nm excitation enhances amide modes, as well as side-chain vibrations of phenylalanine (F) and tyrosine (Y) residues.

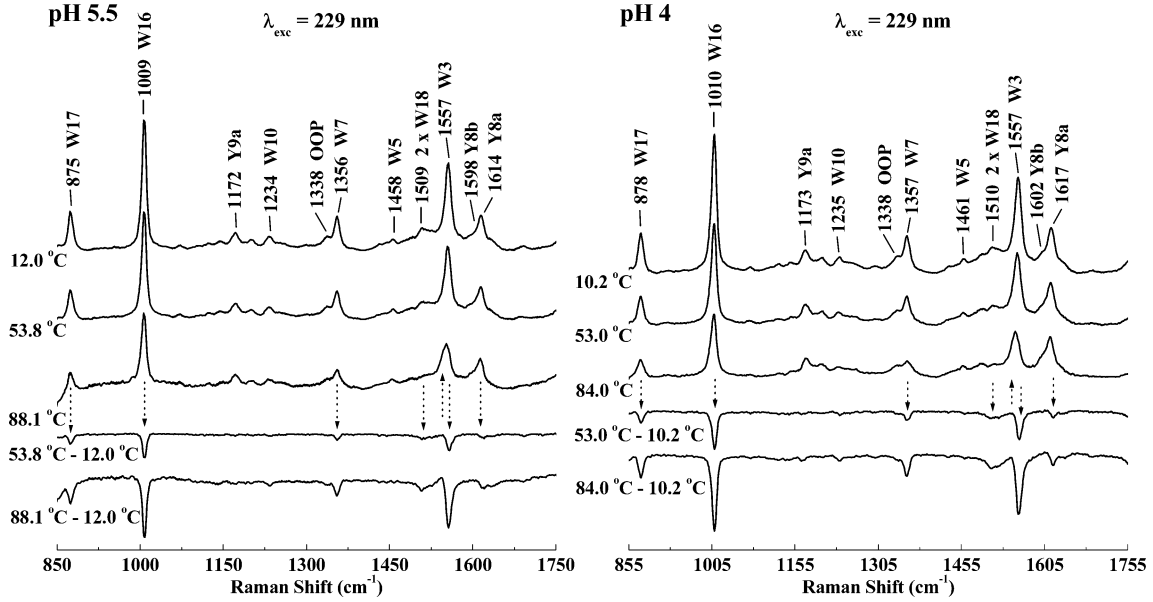

FIGURE 4: Same as Figure 3 but with a 229 nm excitation, which enhances side-chain vibrations of tyrosine (Y) and tryptophan (W) residues.

the tryptophan relaxation, 7 μs, is twice as fast as the phenylalanine and helix-melting relaxations, both of which are ~15 μs. At pH 5.5, however, all of the signals relax at about the same rate.

Table 1 also lists initial (I_0) and long-time ($I_{asymptote}$) signal amplitudes as well as the expected amplitude (I_T) for equilibrium at the final T-jump temperature. The $I_{assymptote}$ and I_T values are in good agreement, showing that the T-jump time range captures the full dynamics and there is no unaccounted slow phase. Also listed is the fractional amplitude for the fast phase, which, in every case, is roughly half of the total amplitude.

DISCUSSION

Structure and Melting. The helix fractions observed via our CD and UVRR measurements, 0.63 and 0.38 at pH 5.5 and 4, are in good agreement with previous determinations (*29*) and are fully consistent with NMR analyses, which reveal a disordered F helix at pH ~6 and a remnant core at pH 4, consisting primarily of the A, G, and H helices. The fraction of residues in helical regions is 0.78 for native myoglobin, of which the F helix accounts for 0.10, while the A, G, and H helices together account for 0.39.

It is reasonable to expect that the A, G, and H helices are also the last to melt as the temperature is raised. However, the pH 5.5 CD melting curve (Figure 7) shows a cooperative transition to a helix fraction of 0.25 or less, with no indication of a pause at 0.40. Thus, at least part of the AGH core melts cooperatively with the more labile B, C, D, and E helices. The melting process monitored by the UVRR amide bands is less cooperative than the CD melting curve at pH 5.5 and retains a higher helix fraction at high temperature. This

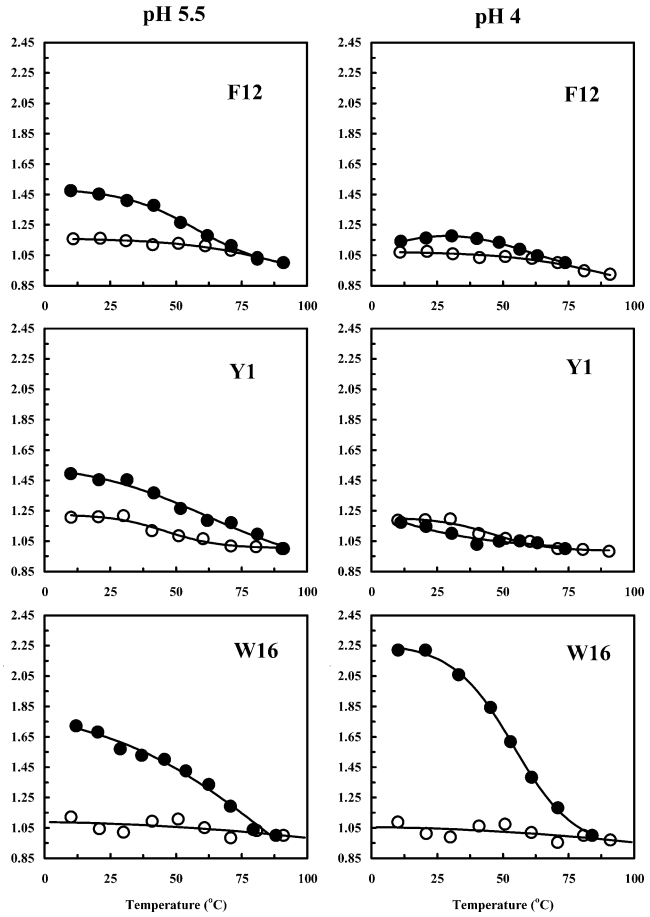

FIGURE 5: Peak heights, normalized to the value at 90 °C, for selected UVRR bands of aromatic residues in apoMb (●) and the appropriate aqueous amino acid (○) at pH 5.5 (left) and 4 (right). (Upper panels) F12 of Phe (1002 cm^{-1}) with a 197 nm excitation. (Middle panels) Y1 of Tyr (852 cm^{-1}) with a 197 nm excitation. (Lower panels) W16 of Trp (1010 cm^{-1}) with a 229 nm excitation.

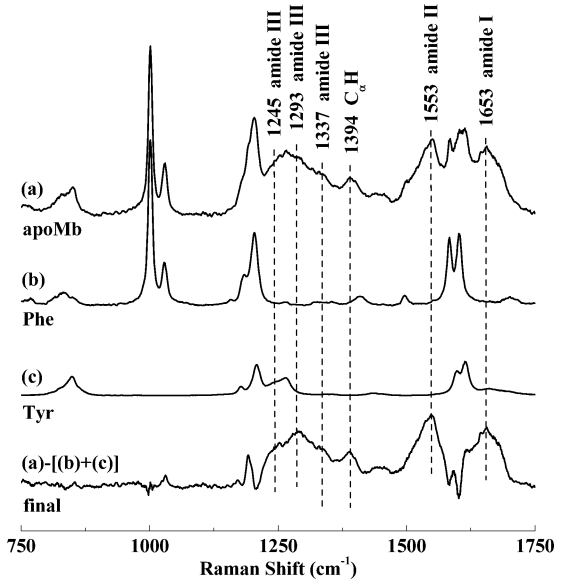

FIGURE 6: Illustration of aromatic interference suppressions in 197-nm-excited apoMb UVRR spectra, by subtraction of aqueous Phe and Tyr spectra.

behavior points to a mechanism in which longer helices melt to shorter helical segments as the temperature is raised; CD is less sensitive to short helices than is UVRR (*28*). At pH

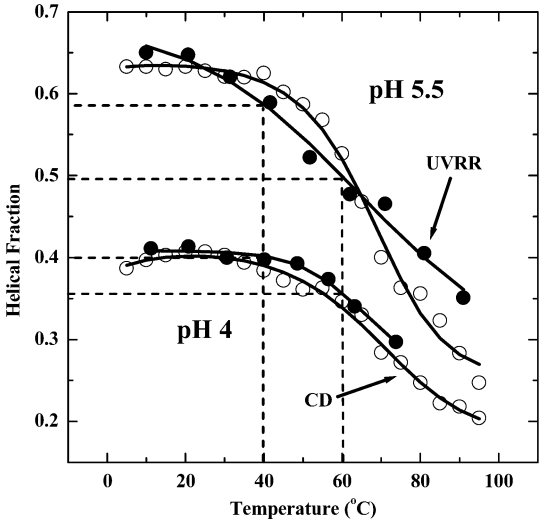

FIGURE 7: Comparison of helix fractions computed via fitting of CD (see the inset of Figure 2) and 197-nm-excited UVRR spectra at the indicated pH values. Expected changes for a 40−60 °C T-jump are indicated.

4, both the CD and UVRR melting curves are less cooperative than at pH 5.5, suggesting greater lability for the helices at low pH, even though they form the AGH core. This observation is consistent with the likely mechanism for acid destabilization of apoMb, namely, protonation of a pair of histidine residues, H24 and H119, whose imidazole rings are buried in the A−B−G−H interface within hydrogen-bonding distance of each other in the holoprotein (*15*). Protonation of the interface renders the helices more fluxional, even if the AGH core persists.

The aromatic residue UVRR signals all show significant exposure to the solvent (Figure 5) in parellel with helix melting, although at pH 4, the tyrosine side chains seem to be fully exposed even at low temperature, judging from the comparable temperature profile for aqueous tyrosine. One tyrosine residue Y146 is near the C terminus of the protein, which is somewhat frayed, even at pH 6 (*14*), and the other is near the N terminus of the G helix (Y103), close to the disordered F helix. Therefore, it is not surprising that both Tyr residues would be solvent-exposed, especially at pH 4. Chi and Asher (*29*) found no change in the Tyr Y8a band UVRR intensity as the apoMb pH was lowered from 6 to 2. There are seven phenylalanine residues, scattered throughout the protein, and the Phe melting curves show a global response, parallel to the helix melting curves.

Both Trp residues are on the A helix, and the side chains are directed into the AGH core. However, the Trp 7 fluorescence band (λ_{max} = 333 nm) is red-shifted from that of Trp 14 (326 nm) and has a 2-fold lower quantum yield at neutral pH, indicative of greater solvent exposure (*30*). Moreover, the Trp 7 flourescence is perturbed between pH 5.5 and 4.3, while the Trp 14 fluorescence is constant, suggesting that the loss of structure further exposes Trp 7 (*30*). Consistent with a differential response of the two residues, the UVRR intensity of the Trp W16 band was found to decrease with a decreasing pH in two stages, with a plateau near pH 4 (*29*, *31*). Hashimoto et al. (*31*) suggested that Trp 14 is exposed first, because, in the native Mb structure, it is protected from the solvent by three leucine side chains from the E helix, which melts at pH 4, but the fluorescence results

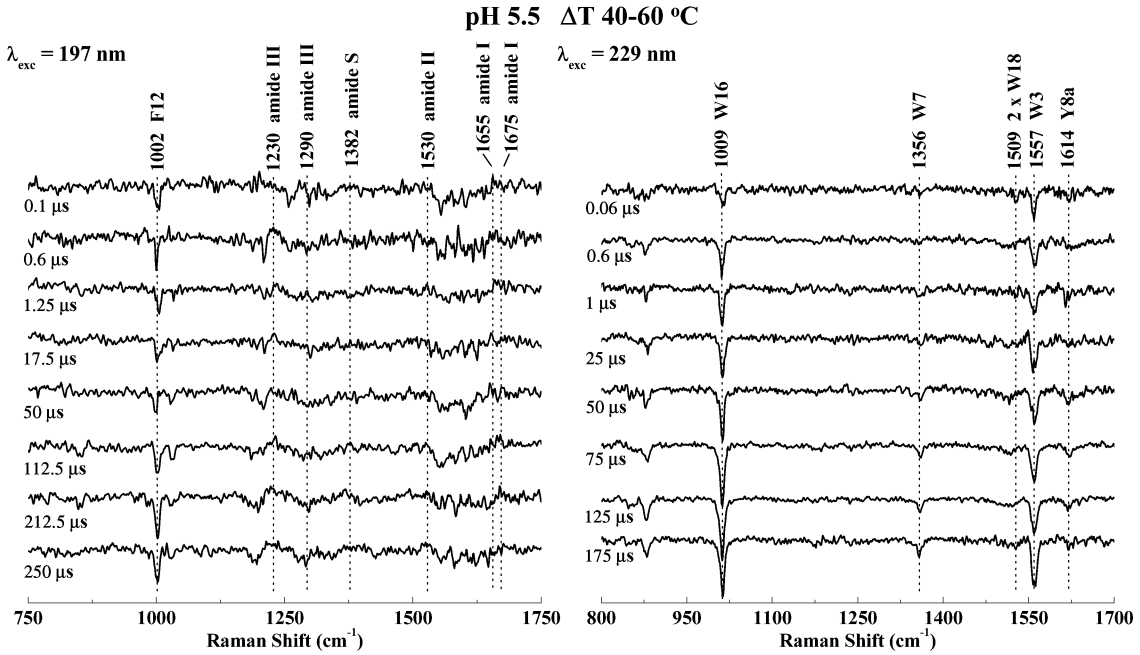

FIGURE 8: UVRR difference spectra with 197 (left) and 229 (right) nm excitations, induced by the indicated T-jump, at the indicated delay intervals, for apoMb at pH 5.5.

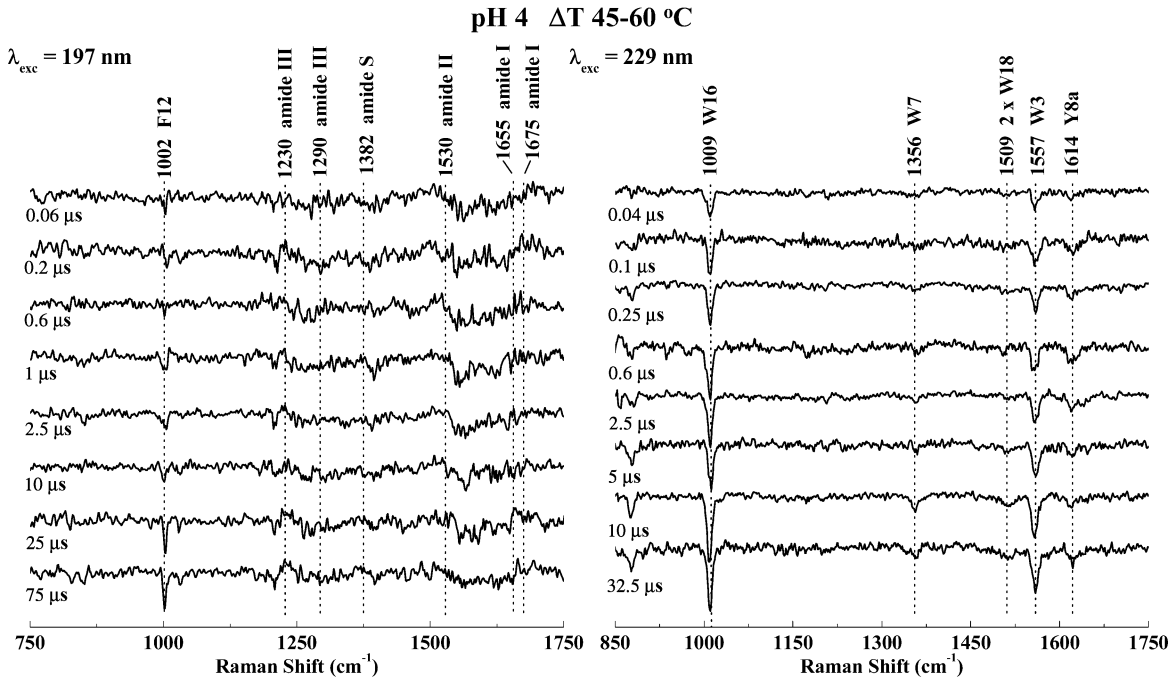

FIGURE 9: Same as Figure 8 but at pH 4.

clearly point to perturbation of Trp 7 in the first stage, as emphasized by Chi and Asher (*29*). The drop in W16 UVRR intensity is larger between pH 4 and 2 than between pH 6 and 4, consistent with our observation of a larger melting decrease at pH 4.0 than at pH 5.5 (Figure 5, bottom). Chi and Asher (*29*) attribute this difference to the greater change in exposed surface area of the more buried Trp 14 than Trp 7. Thus, the evidence points to Trp 14 remaining buried down to pH 4, despite the loss of a stable E helix, and then becoming exposed as the AGH core unravels, at lower pH or higher temperatures.

Dynamics. The T-jump time courses all show a simple and consistent pattern. There is a prompt change, within the instrument time resolution (60 ns), followed by a relaxation on the microsecond time scale. Together, these two phases account for the full amplitude expected from the equilibrium melting curves, for the temperature excursion produced by the T-jump, 40−60 °C at pH 5.5 and 45−60 °C at pH 4. There is no undetected slower process, on the basis of either amide or aromatic residue UVRR signals.

Although the signals monitor unfolding, the relaxations represent the sum of unfolding and folding processes (*1*). Because about half of the helix content is lost at equilibrium at 60 °C (Figure 7), the helix folding and unfolding rates should be about the same, each accounting for half of the observed rate. Dividing the measured rates by two, we

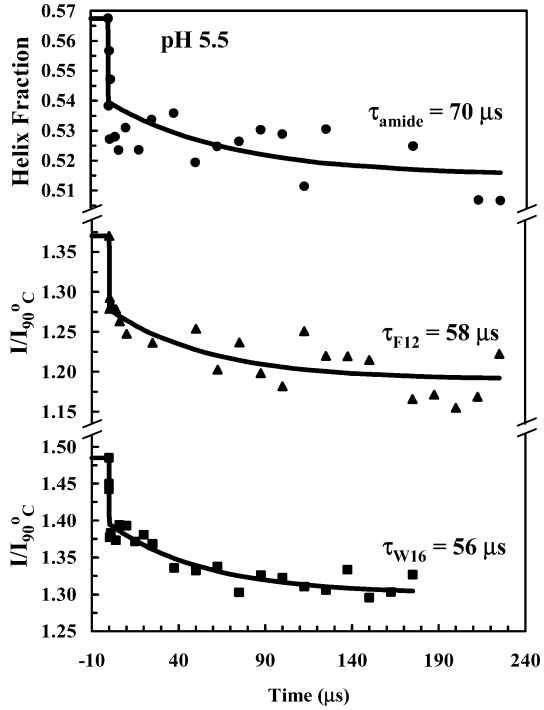

FIGURE 10: UVRR time courses following a 40−60 °C T-jump for apoMb at pH 5.5. (Top panel) Helix fraction from amide band amplitudes (a 197 nm excitation). (Middle panel) Phe F12 peak height, normalized to the 90 °C value (a 197 nm excitation). (Bottom panel) Trp W16 peak height, normalized to the 90 °C value (a 229 nm excitation). The data were fit with an instantaneous change (instrument time limited) followed by an exponential decay, with the indicated time constant.

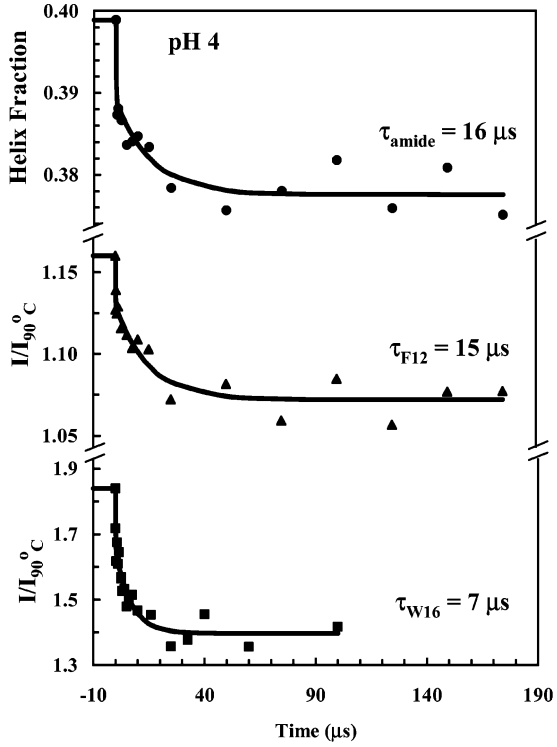

FIGURE 11: Same as Figure 10 but for a 45−60 °C T-jump at pH 4.

estimate 140 and 32 μs as the helix folding time constants at pH 5.5 and 4, although the uncertainties are large. The faster unfolding and refolding at pH 4 is consistent with the greater lability of the AGH core at this pH, probably because of buried histidine protonation, as noted above.

Gilmanshen et al. (*1*) found a 132 μs relaxation for the loss of the apoMb amide I′ IR signal (1659 cm^{-1}) at pD 5.3, about twice as long as our amide UVRR relaxation (70 μs). In view of the experimental uncertainties and of possible differences between H_2O and D_2O solutions, this is quite good agreement. At pD 3 with low salt, Gulotta et al. (*20*) found a 14 μs relaxation for the amide I′ IR signal; the exact agreement with our amide UVRR relaxation (16 μs) at pH 4 is coincidental, in view of the different pH (pD), but both studies demonstrate faster helix folding/unfolding at low pH. However, Gulotta et al. detected a slower amide I′ phase at pH 3, 59 μs, accounting for 40% of the signal (*20*). We see no evidence for this slower phase. Gullota et al. attribute the slower phase to a process leading to a "misformed" AGH core (because a parallel relaxation is not seen for the Trp fluorescence signal, as it is for the faster phase) from a fraction of unfolded molecules, which is farther away from the correct GH hairpin (Figure 1) than the majority of molecules. The absence of a slower phase at pH 4 could then indicate a diminution of this more extended fraction with rising pH.

The aromatic residue UVRR signals provide a separate view of the protein dynamics, responding, as they do, to solvent exposure. We found no T-jump response of the tyrosine signals, consistent with the equilibrium evidence that the two Tyr residues are largely exposed even at low temperature. The phenylalanine bands do show a T-jump response, and the relaxation time constant is the same as that of the amide signal, both at pH 5.5 and 4. This behavior is consistent with the Phe residues being distributed throughout the protein structure, so that the aggregate signal gives a global response.

However, the Trp signals give a clearly individuated response. At pH 5.5, the Trp W16 relaxation time, 56 μs, is indistinguishable from those of the Phe or amide signals, but at pH 4, the Trp relaxation, 7 μs, is twice as fast as that of the Phe or amide signal. At pH 4, the Trp signal is strong, reducing the uncertainty in τ, and the 2-fold acceleration is outside of the experimental error. This signal is assigned to Trp 14, as discussed above. The doubling of the relaxation rate indicates that Trp 14 is exposed to the solvent prior to the melting of the AGH core. Wright and co-workers (private communication) find that, at pH 4 or in the corresponding folding intermediate, the H helix is translated, relative to its position in native apoMb. This shift might loosen the packing around the Trp 14 side chain and allow excursions which are faster than helix melting. We note that Gullota et al. (*20*) found the same relaxation time for tryptophan fluorescence as for the helix IR signal at pH 3. The absence of Trp acceleration, relative to the helix, might indicate a change in the mechanism at pH 3, or it might reflect the differing sensitivities of the UVRR intensity, which depends upon solvent exposure, and the fluorescence yield, which depends upon quenching, a longer range mechanism.

At pH 5.5, the UVRR response is attributed to Trp 7, which is already somewhat solvent-exposed at low temperatures. Its further exposure parallels the global helix melting and Phe exposure transients; there is no acceleration of the Trp relaxation, as there is at pH 4.

Table 1: Time-Course Parameters Following T-jumps at pH 5.5 (40−60 °C) and pH 4.0 (45−60 °C)

		pH 5.5					pH 4				
λ	signal	I_0[a]	I_T[b]	$I_{asymptote}$[c]	% fast[d]	τ (μs)[e]	I_0	I_T	$I_{asymptote}$	% fast	τ (μs)
197 nm	amide	0.567	0.516	0.501	53	70 ± 53	0.399	0.377	0.365	46	16 ± 9
	F12	1.37	1.19	1.20	51	58 ± 35	1.16	1.07	1.06	35	15 ± 5
229 nm	W16	1.49	1.30	1.33	49	56 ± 21	1.84	1.40	1.42	43	7 ± 2

[a] I_0, initial intensity (40 or 45 °C) relative to 90 °C, for the indicated aromatic band or helix fraction for the amide signal. [b] I_T, 60 °C intensity or helix fraction. [c] $I_{asymptote}$, intensity or helix fraction approached asymptotically in the exponential phase. [d] Percentage of the total change occurring in the instantaneous phase. [e] Time constant for the exponential phase, with indicated uncertainty.

We now turn to the nature of the instrument-limited prompt response to the T-jump, which accounts for about half the amplitude for all of the signals. In the case of the aromatic residue signals, this result implies that there is rapid exposure to the solvent, prior to the unfolding phase. We attribute this phenomenon to solvent penetration into the protein, in response to a heat pulse. Solvation and desolvation is recognized to be a critical aspect of protein folding (*32*), and recent simulations (*33*) as well as experimental findings (*34*, *35*) indicate that folding occurs via the collapse to a structured but hydrated state, followed by cooperative exclusion of the remaining water. We propose that the prompt response of the aromatic residue signals represent the reverse of this process, with water squeezing into the structure prior to unfolding. This happens on the nanosecond time scale.

The prompt response of the amide UVRR signals probably corresponds to the ~40 ns relaxation measure by Gilmanshin et al. (*1*, *36*) for an infrared transient of apoMb at pD 5.3 or 3, measured at 1632 cm^{-1}, a frequency assigned to hydrated helical elements. The transient was suggested to arise from folding/unfolding of hydrated helices. In contrast to the IR amide I signal, there is no clear indication in the Raman spectrum of whether the helix is hydrated or not. In the Raman optical activity (ROA) spectrum, a 1344 cm^{-1} band has been assigned to hydrated helix (*37*), but the Raman signal from this band seems to be too weak for detection. The secondary structure sensitivity of the Raman spectrum resides mainly in the amide III band (*13*), which may not be sensitive to solvation (because the mode does not involve C═O stretching). Thus, the prompt melting behavior detected via the UVRR amide bands may well reflect melting of hydrated helices. Because the hydrated helices are attributed to already exposed segments in the protein structure, their melting is unrelated to solvent penetration into the protein interior. The coincidence of the prompt helix and aromatic residue responses merely reflects the instrumental resolution.

CONCLUSIONS

Because multiple structural probes are provided, UVRR spectroscopy can provide a more complete picture than has previously been available for the mechanisms of protein folding. In particular, the signals from aromatic residues monitor tertiary contacts, while the amide signals report on backbone conformation. Measuring both signals can answer the question whether tertiary contacts precede or follow formation of secondary structure.

The present results uncover a clear differentiation of helix melting and tertiary contact formation in the case of the AGH core of the apoMb-folding intermediate at pH 4. A key side chain within this core, that of Trp14, responds to a T-jump twice as fast as does helix melting. Thus, Trp14 loses its tertiary contacts prior to melting of the AGH core. It follows that in the folding direction, the helices must form prior to their final rearrangement, which allows proper formation of tertiary contacts (*38*), at least in the case of Trp14. While this kind of mechanism has previously been anticipated, the UVRR time courses provide direct evidence.

The aromatic residue UVRR signals also probe access of the solvent to the side chains. In the case of phenylalanine, this is the only mechanism for changing the signal, because the phenyl ring is unable to form hydrogen bonds to acceptor residues, unlike the tyrosine and tryptophan side chains. Thus, the phenylalanine UVRR bands provide a direct measure of solvent exposure. The fact that half of the Phe response (as well as half of the Trp response) to a T-jump occurs within the first 60 ns provides strong evidence for the role of solvent penetration as the precursor to protein unfolding. Solvent penetration is the microscopic reverse of solvent exclusion, which is indicated by modeling studies to be the final event in protein folding.

ACKNOWLEDGMENT

We thank Prof. Peter Wright for helpful discussions.

REFERENCES

1. Gilmanshin, R., Williams, S., Callender, R. H., Woodruff, W. H., and Dyer, R. B. (1997) Fast events in protein folding: Relaxation dynamics of secondary and tertiary structure in native apomyoglobin, *Proc. Natl. Acad. Sci. U.S.A. 94*, 3709−3713.
2. Huang, C.-Y., Getahun, Z., Zhu, Y. J., Klemke, J. W., DeGrado, W. F., and Gai, F. (2002) Helix formation via conformation diffusion search, *Proc. Natl. Acad. Sci. U.S.A. 99*, 2788−2793.
3. Ballew, R. M., Sabelko, J., and Gruebele, M. (1996) Direct observation of fast protein folding: The initial collapse of apomyoglobin, *Proc. Natl. Acad. Sci. U.S.A. 93*, 5759−5764.
4. Thompson, P. A., Eaton, W. A., and Hofrichter, J. (1997) Laser temperature jump study of the helix−coil kinetics of an alanine peptide interpreted with a "kinetic zipper" model, *Biochemistry 36*, 9200−9210.
5. Lednev, I. K., Karnoup, A. S., Sparrow, M. C., and Asher, S. A. (1999) Nanosecond UV resonance Raman examination of initial steps in α-helix secondary structure evolution, *J. Am. Chem. Soc. 121*, 4076−4077.
6. Fodor, S. P. A., Copeland, R. A., Grygon, C. A., and Spiro, T. G. (1989) Deep-ultraviolet Raman excitation profiles and vibronic scattering mechanisms of phenylalanine, tyrosine, and tryptophan, *J. Am. Chem. Soc. 111*, 5509−5518.
7. Copeland, R. A., and Spiro, T. G. (1987) Secondary structure determination in proteins from deep (192−223 nm) ultraviolet Raman spectroscopy, *Biochemistry 26*, 2134−2139.
8. Austin, J. C., Rodgers, K. R., and Spiro, T. G. (1993) Protein structure from ultraviolet resonance Raman spectroscopy, *Methods Enzymol. 226*, 374−396.
9. Balakrishnan, G., Hu, Y., and Spiro, T. G. (2005) *Appl. Spectrosc.* (submitted).
10. Zhao, X. J., Chen, R. P., Tengroth, C., and Spiro, T. G. (1999) Solid-state tunable kHz ultraviolet laser for Raman applications, *Appl. Spectrosc. 53*, 1200−1205.

11. Zhao, X. J., Tengroth, C., Chen, R. P., Simpson, W. R., and Spiro, T. G. (1999) Time-resolved Raman spectroscopy with a tunable ultraviolet kilohertz nanosecond laser, *J. Raman Spectrosc. 30*, 773−776.
12. Balakrishnan, G., Hu, Y., Nielsen, S. B., and Spiro, T. G. (2005) Tunable kHz deep ultraviolet (193−210 nm) laser for Raman applications, *Appl. Spectrosc. 59*, 776−781.
13. Huang, C.-Y., Balakrishnan, G., and Spiro, T. G. (2005) Protein secondary structure from deep UV resonance Raman spectroscopy, *J. Raman Spectrosc.* (in press).
14. Eliezer, D., and Wright, P. E. (1996) Is apomyoglobin a molten globule? Structural characterization by NMR, *J. Mol. Biol. 263*, 531−538.
15. Lecomte, J. T. J., Kao, Y. H., and Cocco, M. J. (1996) The native state of apomyoglobin described by proton NMR spectroscopy: The A−B−G−H interface of wild-type sperm whale apomyoglobin, *Proteins 25*, 267−285.
16. Gilmanshin, R., Dyer, R. B., and Callender, R. H. (1997) Structural heterogeneity of the various forms of apomyoglobin: Implications for protein folding, *Protein Sci. 6*, 2134−2142.
17. Eliezer, D., Chung, J., Dyson, H. J., and Wright, P. E. (2000) Native and non-native secondary structure and dynamics in the pH 4 intermediate of apomyoglobin, *Biochemistry 39*, 2894−2901.
18. Hughson, F. M., Wright, P. E., and Baldwin, R. L. (1990) Structural characterization of a partly folded apomyoglobin intermediate, *Science 249*, 1544−1548.
19. Eliezer, D., Yao, J., Dyson, H. J., and Wright, P. E. (1998) Structural and dynamic characterization of partially folded states of apomyoglobin and implications for protein folding, *Nat. Struct. Biol. 5*, 148−155.
20. Gulotta, M., Gilmanshin, R., Buscher, T. C., Callender, R. H., and Dyer, R. B. (2001) Core formation in apomyoglobin: Probing the upper reaches of the folding energy landscape, *Biochemistry 40*, 5137−5143.
21. Teale, F. W. J. (1959) Cleavage of the haem-protein link by acid methylethyl ketone, *Biochim. Biophys. Acta 35*, 543−543.
22. Rothgeb, T. M., and Gurd, F. R. N. (1978) Physical methods for the study of myoglobin, *Methods Enzymol. 52*, 473−486.
23. Edelhoch, H. (1967) Spectroscopic determination of tryptophan and tyrosine in proteins, *Biochemistry 6*, 1948−1954.
24. Sreerama, N., and Woody, R. W. (2000) Estimation of protein secondary structure from circular dichroism spectra: Comparison of CONTIN, SELCON, and CDSSTR methods with an expanded reference set, *Anal. Biochem. 287*, 252−260.
25. Anfinrud, P. A., Han, C., and Hochstrasser, R. M. (1989) Direct observations of ligand dynamics in hemoglobin by subpicosecond infrared spectroscopy, *Proc. Natl. Acad. Sci. U.S.A. 86*, 8387−8391.
26. Gilmanshin, R., Gulotta, M., Dyer, R. B., and Callender, R. H. (2001) Structures of apomyoglobin's various acid-destabilized forms, *Biochemistry 40*, 5127−5136.
27. Woody, R. W. (1996) in *Circular Dichroism and the Conformational Analysis of Biomolecules* (Fasman, G. D., Ed.) pp 25−68, Plenum Press, New York.
28. Ozdemir, A., Lednev, I. K., and Asher, S. A. (2002) Comparison between UV Raman and circular dichroism detection of short α helices in Bombolitin III, *Biochemistry 41*, 1893−1896.
29. Chi, Z. H., and Asher, S. A. (1999) Ultraviolet resonance Raman examination of horse apomyoglobin acid unfolding intermediates, *Biochemistry 38*, 8196−8203.
30. Postnikova, G. B., Komarov, Y. E., and Yumakova, E. M. (1991) Fluorescence study of the conformational properties of myoglobin structure. 1. pH-dependent changes of tryptophanyl fluorescence in intact and chemically modified sperm whale apomyoglobins, *Eur. J. Biochem. 198*, 223−232.
31. Hashimoto, S., Fukasaka, J., and Takeuchi, H. (2001) Structural study on acid-induced unfolding intermediates of myoglobin by using UV resonance Raman scattering from tryptophan residues, *J. Raman Spectrosc. 32*, 557−563.
32. Fersht, A. R. (1999) *Structure and Mechanism in Protein Science: A Guide to Enzyme Catalysis and Protein Folding*, W. H. Freeman, New York.
33. Cheung, M. S., Garcia, A. E., and Onuchic, J. N. (2002) Protein folding mediated by solvation: Water expulsion and formation of the hydrophobic core occur after the structural collapse, *Proc. Natl. Acad. Sci. U.S.A. 99*, 685−690.
34. Zhang, O. W., and Forman-Kay, J. D. (1997) NMR studies of unfolded states of an SH3 domain in aqueous solution and denaturing conditions, *Biochemistry 36*, 3959−3970.
35. Mok, Y. K., Kay, C. M., Kay, L. E., and Forman-Kay, J. (1999) NOE data demonstrating a compact unfolded state for an SH3 domain under non-denaturing conditions, *J. Mol. Biol. 289*, 619−638.
36. Jones, C., Henry, E., Hu, Y., Chan, C., Luck, S., Bhuyan, A., Roder, H., Hofrichter, J., and Eaton, W. (1993) Fast events in protein folding initiated by nanosecond laser photolysis, *Proc. Natl. Acad. Sci. U.S.A. 90*, 11860−11864.
37. Blanch, E. W., Bell, A. F., Hecht, L., Day, L. A., and Barron, L. D. (1999) Raman optical activity of filamentous bacteriophages: Hydration of α-helices, *J. Mol. Biol. 290*, 1−7.
38. Kim, P. S., and Baldwin, R. L. (1982) Specific intermediates in the folding reactions of small proteins and the mechanism of protein folding, *Annu. Rev. Biochem. 51*, 459−489.
39. Humphrey, W., Dalke, A., and Schulten, K. (1996) VMD: Visual molecular dynamics, *J. Mol. Graphics 14*, 33−38.

BI051578U